

# Mathematical modeling and numerical analysis of intermediate-temperature water (steam) electrolysis cell performances

*Sergey Grigoriev*<sup>1,2,3,4\*</sup>, and *Alexander Kalinnikov*<sup>2</sup>

<sup>1</sup> National Research University “Moscow Power Engineering Institute”, 111250 Moscow, Russia

<sup>2</sup> National Research Center “Kurchatov Institute”, 123182 Moscow, Russia

<sup>3</sup> A.N. Nesmeyanov Institute of Organoelement Compounds of the Russian Academy of Sciences, 119334 Moscow, Russia

<sup>4</sup> HySA Infrastructure Center of Competence, North-West University, Potchefstroom 2531, South Africa

**Abstract.** A physicochemical model of an intermediate-temperature water (steam) electrolyzer based on a proton exchange membrane (PEM) was developed. The results of numerical modeling provide recommendations for membrane-electrode assembly (MEA) parameters based on the required electrolyzer operating conditions. Specifically, electrocatalytic layer thicknesses can be recommended to ensure high electrolyzer performance with optimal platinum metals content. The importance of sufficient ionomer in the electrocatalytic layers is demonstrated.

---

\* Corresponding author: [sergey.grigoriev@outlook.com](mailto:sergey.grigoriev@outlook.com)

## 1 Introduction

Proton exchange membrane (PEM) water electrolyzers have been successfully used for decades in industry, particularly in the energy sector, for generating high-purity hydrogen and oxygen [1-2]. Despite their utility, low-temperature PEM electrolyzers face significant hurdles: high energy consumption for gas production (approximately 5 kWh/m<sup>3</sup> of hydrogen), stringent high requirements for water purity (conductivity of less than 0.1 μS/cm), and the expense of polymer membranes like Nafion®. These limitations result in substantial capital and operational costs, hindering the broad implementation of low-temperature PEM technology. A key strategy to overcome these issues is to perform intermediate-temperature electrolysis of water/steam at temperatures increased up to 180-200°C.

Intermediate-temperature PEM electrolysis is favored due to improved kinetics, thermodynamics, and process engineering [3]. Higher temperatures boost electrode reaction speeds, notably the oxygen evolution reaction (OER), which is the most energy-demanding process, thereby reducing polarization losses. Elevated electrolysis temperatures also decrease the reversible voltage, leading to lower thermodynamic losses. Therefore, intermediate-temperature steam electrolysis offers a more energy-efficient pathway for producing electrolysis gases compared to traditional low-temperature processes (below 100°C). Moreover, utilizing alternative high-temperature proton-conducting membranes that exhibit reduced susceptibility to water contaminants than perfluorinated membranes like Nafion® and Aquivion®, simplifies water management. This allows for the use of steam produced by generators or evaporators instead of highly purified water. Engineering-wise, higher operating temperatures in electrolysis modules can simplify cooling systems, particularly under conditions of elevated current density. Heat exchange is driven by the temperature differential between the electrolyzer and its surroundings. Operating at elevated temperatures facilitates the design of more efficient and compact cooling systems. For instance, an increase from 80 to 160°C can lead to a three- to four-fold reduction in the required heat exchanger radiator area. Furthermore, in specific cases where electrolysis voltages are low (below the thermoneutral point), low-grade heat sources such as geothermal energy [4] or industrial/nuclear waste heat [5] can be harnessed.

Some attempts to use various intermediate-temperature membrane materials and electrolyte solutions have been realized. For example, 0.1-0.2 mm thick sheets produced from SiC powder bound with a small amount of PTFE have been used as a matrix in [6].

So-called solid acid electrolysis cells with CsH<sub>2</sub>PO<sub>4</sub> used as an electrolyte has been reported in [7-9]. The phosphoric-acid-doped polyvinyl chloride (PVC)-poly(4-vinylpyridine) (P4VP) hybrid membrane was applied in the temperature range of 100–180°C in [10]. However, the main membrane matrix/electrolyte widely used is polybenzimidazole (PBI) doped with phosphoric acid (PA) to ensure proton conductivity.

Since the water electrolyzer using the PBI-PA system is a relatively novel device, optimization of the membrane-electrode assembly (MEA) parameters and modes of electrolyzer operation is needed. Using mathematical simulation proves to be a valuable method for addressing the aforementioned problem [11].

Our work here outlines developed physicochemical model and the numerical analyses performed on PBI-PA-based MEA. Special attention is given to the numerical analysis of the distribution of potentials and currents, both for electrons and protons, across the MEA.

## 2 Mathematical model and numerical technique

### 2.1 Model description and assumptions

The model considers all electrolysis cell components (as schematically shown in Fig. 1) separately, with their interactions defined by the boundary conditions.

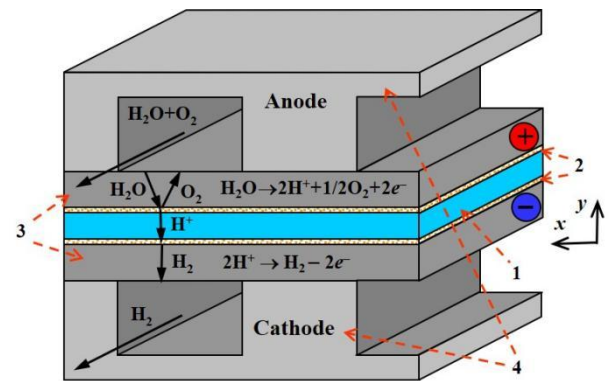


**Fig. 1.** A schematic overview of a PEM water electrolyzer single cell. 1 – PBI-PA membrane; 2 – catalytic layers; 3 – gas diffusion electrodes/current collectors; 4 – bipolar plates.

The model simulates:

- the movement of steam and electrolytic gases in the bipolar plate channels, gas diffusion electrodes, catalytic layers;
- protons movement within the membrane and electrocatalytic layers;
- electrons flow in the catalytic layer and gas diffusion electrodes, and through the bipolar plate's current transfer ribs;
- heat transfer throughout all components.

Key assumptions underpinning the model include:

- steady-state operation of the electrolyzer;
- incompressible, ideal gas flows at constant pressure in the bipolar plate channels;
- absence of axial gas velocity in the gas diffusion electrodes;
- equal pressures in the cathode and anode compartments;
- constant pressure for all mass transfer phenomena;

- the contacting surfaces of the bipolar plates and the gas diffusion electrodes have identical temperatures and are equipotential;
- within the gas diffusion electrodes, the potential is considered to be constant, varying solely along the y-axis;
- the water vapor flows in the bipolar plate channel are assumed to be laminar (Reynolds number < 1000);
- anhydrous Grotthuss-type transport mechanism of protons transport in PBI-PA membrane;
- membrane, electrocatalytic layers, and gas diffusion electrodes are isotropic and uniform.

## 2.2 The fundamental mathematical descriptions and their constraints

Table 1 presents a summary of the fundamental equations that form the basis of the mathematical model.

**Table 1.** Equations used in the mathematical model

Equation type	Electrolyzer regions
Navier–Stokes equations (equations of motion) alongside the continuity equation	Bipolar plate, gas diffusion electrodes and catalytic layers
Stephan–Maxwell relations	Gas diffusion electrodes
Nernst–Planck equation governing ionic transport through PBI-PA	Membrane, electrocatalytic layers
Convective-diffusion equation accounting for both diffusion and convection (Fick’s law with convection)	Bipolar plate, gas diffusion electrodes, electrocatalytic layers
Transport equations for electric charge and gaseous phase dynamics	Gas diffusion electrodes, electrocatalytic layers
Nernst equation and Butler–Volmer kinetics	Electrocatalytic layers

Quasi-stationary gas flow distribution in bipolar plate channels was governed by the Navier–Stokes equation:

$$\begin{cases} \rho v_x \frac{\partial v_x}{\partial x} + \rho v_y \frac{\partial v_x}{\partial y} + \rho v_z \frac{\partial v_x}{\partial z} + \mu \nabla^2 v_x = \frac{\partial p}{\partial x} \\ \rho v_x \frac{\partial v_y}{\partial x} + \rho v_y \frac{\partial v_y}{\partial y} + \rho v_z \frac{\partial v_y}{\partial z} + \mu \nabla^2 v_y = \frac{\partial p}{\partial y} \\ \rho v_x \frac{\partial v_z}{\partial x} + \rho v_y \frac{\partial v_z}{\partial y} + \rho v_z \frac{\partial v_z}{\partial z} + \mu \nabla^2 v_z = \frac{\partial p}{\partial z} \\ \frac{\partial v_x}{\partial x} + \frac{\partial v_y}{\partial y} + \frac{\partial v_z}{\partial z} = 0 \\ a \leq x \leq a+b \quad 0 \leq y \leq h \quad 0 \leq z \leq L \end{cases}$$

where  $\mu$  is the dynamic viscosity of the gas medium of the channel,  $b \cdot h$  is the channel cross-section,  $L$  is the channel length,  $a$  and  $b$  are width of rib and channel, respectively, operator  $\nabla^2 = \frac{\partial^2}{\partial x^2} + \frac{\partial^2}{\partial y^2} + \frac{\partial^2}{\partial z^2}$ .

Diffusion processes in a multicomponent medium are expressed by the Stefan–Maxwell equations:

$$\begin{cases} C_g \nabla c_1 = \frac{c_1 \mathbf{N}_2 - c_2 \mathbf{N}_1}{D_{12}} \\ C_g \nabla c_2 = -\frac{c_1 \mathbf{N}_2 - c_2 \mathbf{N}_1}{D_{12}} \\ \varepsilon \frac{\partial}{\partial t} [(1-s)c_1] + \nabla \mathbf{N}_1 + Q_1 = 0 \\ \varepsilon \frac{\partial}{\partial t} [(1-s)c_2] + \nabla \mathbf{N}_2 + Q_2 = 0 \end{cases}$$

where  $D_{ij}$  is denotes the binary diffusion coefficient for components  $i$  and  $j$ ;  $Q_i$  is the specific power of the volume source of component  $i$ .

The mass conservation of the gas phase is expressed as follows:

$$\frac{\partial}{\partial t} [(1-s)C_g \varepsilon] + \nabla (C_g \mathbf{v}_g) + Q_g = 0$$

where  $\varepsilon$  – medium porosity.

Momentum is conserved in the gas phase when the forces that resist its flow are equal to the pressure gradients of each phase, a relationship explained by Darcy’s law:

$$\nabla P_g = -\lambda_g \mathbf{v}_g \quad \lambda_g = \frac{\mu_g}{K_p k_{rg}} = \frac{\mu_g}{K_p (1-s)^3}$$

where  $K_p$  is the Darcy coefficient,  $P_g$  is the gas pressure.

Charge transfer processes associated with electrochemical reactions are considered in accordance with the Laplace equation:

$$\frac{\partial}{\partial x} \left( \sigma_{xx} \frac{\partial \varphi}{\partial x} \right) + \frac{\partial}{\partial y} \left( \sigma_{yy} \frac{\partial \varphi}{\partial y} \right) + \frac{\partial}{\partial z} \left( \sigma_{zz} \frac{\partial \varphi}{\partial z} \right) = S_I$$

where  $\varphi$  is the potential,  $\sigma_{ii}$  is the diagonal components of the conductivity tensor,  $S_I$  is the current absorption due to electrochemical reactions.

The proton current in the membrane and electrocatalytic layer was calculated from the Nernst–Planck equation:

$$J_i = -D_i \nabla c_i - z_i c_i \frac{F}{RT} \nabla \varphi$$

where  $J_i$ ,  $D_i$ ,  $c_i$  and  $z_i$  are respectively the current density, diffusion coefficient, molar concentration and charge of ion  $i$ ;  $F$  is the Faraday constant;  $R$  – universal gas constant;  $T$  – temperature;  $\varphi$  – electrical potential.

The boundary conditions for all potentials  $\varphi$  of flows  $N$  within the MEA’s cross-section are consistently expressed as:

$$\begin{cases} y = 0 \quad 0 \leq x \leq a+b \quad N_y = F(x) \quad \frac{\partial \varphi}{\partial y} = F(x) \\ 0 \leq y \leq h_g \quad x = 0, a+b \quad N_x = 0 \quad \frac{\partial \varphi}{\partial x} = 0 \\ y = h_g \quad 0 \leq x \leq a \quad N_y = 0 \quad \frac{\partial \varphi}{\partial y} = 0 \\ 0 \leq y \leq h_g \quad a \leq x \leq a+b \quad N_x = 0 \quad \frac{\partial \varphi}{\partial x} = 0 \end{cases}$$

where  $h_g$  is gas diffusion electrode thickness.

Therefore, the only distinction in the boundary conditions across all the flows occurs at the  $y = 0$  plane, which corresponds to the electrocatalytic layer.

The general equation of heat distribution in the layers of the electrolyzer is used as follows:

$$C_p \frac{\partial T}{\partial t} = -\nabla H + W_0,$$

where  $H$  - enthalpy flow;  $W_0$  - heat sources in the electrolyzer area under consideration;  $C_p$  - specific heat capacity of the porous medium.

The mathematical framework is thoroughly detailed in [12].

### 2.3 Numerical technique

The alternating direction method was selected as the numerical technique for solving each two-dimensional equation on the space grid. The authors developed custom software, utilizing a grid method, to compute the numerical solution for the system of equations.

### 2.4 Initial data for calculations

Below are the fundamental components, parameters, and operational conditions employed in calculations.

Electrocatalyst layers were characterized by their specific electrochemically active surface area and the specific content of active components (IrO<sub>2</sub> and Pt/C). The anode and cathode catalyst layers are characterized by:

- platinum and iridium oxide specific content: 1 m<sup>2</sup>/g each;
- porosity: 0.4;
- permeability: 1 x 10<sup>-14</sup> m<sup>2</sup>;
- contact angle: 76°;
- platinum mass fraction in catalyst: 0.4;
- iridium specific active surface area per unit mass: 10 m<sup>2</sup>/g;
- polymer electrolyte volume fraction in catalyst layer: 0.2.

Gas diffusion electrodes (anode and cathode) exhibit:

- thickness: 0.3 mm;
- porosity: 0.25 for the anode and 0.7 for the cathode;
- permeability: 1 x 10<sup>-14</sup> m<sup>2</sup>;
- contact angle: 70°.

Membrane specifications include:

- thickness: 150 μm.
- proton conductivity (for PBI with 11 mol/l orthophosphoric acid doping): 6.7 x 10<sup>-3</sup> S/cm.

Operational parameters are:

- pressure: 0.1 MPa;
- temperature: 160°C.

## 3 Results and discussions

Typical results of numerical calculations are shown in Fig. 2. The upper graph refers to the transport of charge carriers (currents of protons and electrons). The other, the lower graph, shows the distribution of electron and proton potentials, including overvoltages. The area of the cathodic electrocatalytic layer is marked in green, and the anodic electrocatalytic layer in blue. The membrane area (between the electrocatalytic layer) has been artificially reduced.

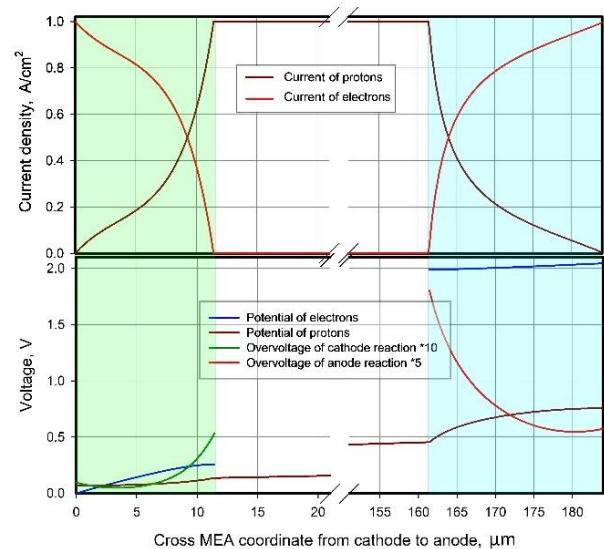


**Fig. 2.** Distribution of potentials and currents of protons and electrons across the MEA.

Analysis of the numerical results shown in Fig. 2 revealed the following. It can be concluded that both the cathodic and anodic electrocatalytic layers function uniformly throughout their thickness. At the same time, electrochemical reactions at both the cathode and anode are somewhat shifted toward the near-membrane region of the catalyst layer (sections near the gas diffusion electrodes operate less efficiently). This phenomenon also occurs in model calculations of operating parameters of low-temperature electrolyzers on the basis of Nafion® membranes [12], although it is less pronounced in electrocatalytic layers containing Nafion® ionomer. It can be assumed that this is a result of the weak proton conductivity of both the cathode and anodic electrocatalytic layers, resulting from the use of a different ionomer (PBI) [13]. The change in electron potential at the cathode is more significant than at the anode (0.25 V at the cathode and less than 0.1 V at the anode), which can be explained by the high electrical resistance of the cathode electrocatalytic layer, which contains carbon particles, which have a higher resistance compared to iridium oxide. Conversely, the change in proton potential is greater at the anode than at the cathode (0.6 V at the anode and 0.1 V at the cathode), which can be explained by the lower polymer electrolyte content at the anode. The overpotential of the anodic reaction is an order of magnitude higher than the overpotential of the cathodic reaction, which is generally typical for water electrolysis.

In general, calculations show that it is advisable to use anodic electrocatalytic layers 10-15 μm thick. This thickness will ensure the required anodic reaction characteristics. For the cathode, an active layer thickness of 7-10 μm is sufficient.

The primary factors contributing to potential losses are the activation losses occurring within the anode electrocatalytic layer, given that the overpotential for the oxygen evolution reaction (OER) is significantly greater than that for the hydrogen evolution reaction

(HER). Additionally, ohmic losses play a minor role. Overall, these potential losses increase almost linearly with the current density.

Based on the operating parameters listed in p. 2.4, the current-voltage characteristics shown in Fig. 3 were calculated.

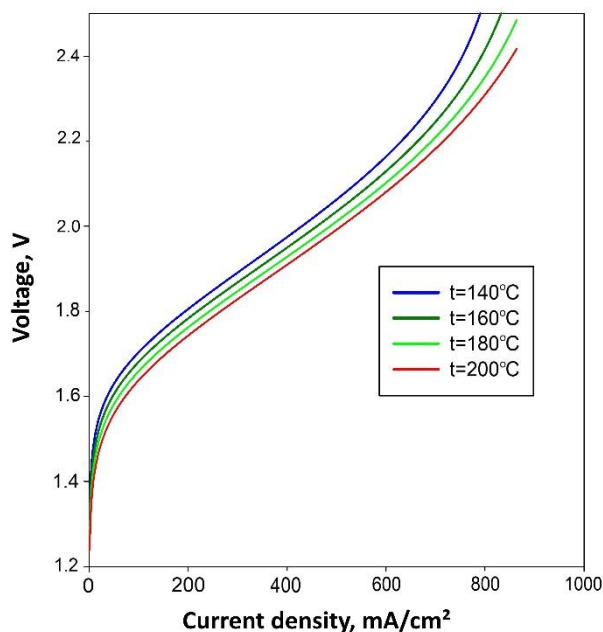


**Fig. 3.** Current-voltage curves at different temperatures of electrolysis cell.

Figure 3 clearly illustrates that the average current density reaches  $0.5 \text{ A/cm}^2$  when the voltage is set to *ca.* 2 V, which is in a good agreement with experimental data [14], taking into consideration almost 2 times difference in PBI-PA membrane thickness. With increasing temperature, the membrane conductivity improves, and the overpotential of the electrode reactions also decreases somewhat, resulting in a decrease in the electrolysis voltage. The obtained dependences are in qualitative agreement with the data of [10].

## 4 Conclusions

The development of a physicochemical model for an intermediate-temperature PEM water (steam) electrolyzer was undertaken. Numerically calculated current-voltage curves of electrolysis cell are in a good agreement with experimental data. The numerical results of this study can be used to make recommendations for MEA parameters, depending on the electrolyzer operating modes. In particular, since OER is the most energy-consuming process, according to calculations, the thickness of the anode electrocatalytic layer should be approximately 2 times greater than the thickness of the cathode layer responsible for HER, which occurs with minimal overvoltage. The presence of an ionomer with high thermal-oxidative stability plays a critical role in achieving high performance of electrocatalytic layers.

The study was supported by the Russian Science Foundation, grant no. 25-29-00545, <https://rscf.ru/project/25-29-00545/>.

## References

1. S.A. Grigoriev, Encyclopedia of Electrochemical Power Sources, Ed. by J. Garche (Elsevier, 2025), p. 65. <https://doi.org/10.1016/B978-0-323-96022-9.00173-0>
2. P. Millet, S. Grigoriev, V. Porembskiy Development and characterisation of a pressurized PEM bi-stack electrolyzer. International Journal of Energy Research. **37**, 449 (2013). DOI: 10.1002/er.2916
3. S.A. Grigoriev, Intermediate-Temperature Water Electrolyzers with a Polymer Membrane: Current Status and Prospects. Nanobiotechnology Reports. **20**, 381 (2025). doi:10.1134/S263516762560021X.
4. J. Sigurvinsson, C. Mansilla, P. Lovera, F. Werkoff, Can high temperature steam electrolysis function with geothermal heat? International Journal of Hydrogen Energy **32**, 1174 (2007). <https://doi.org/10.1016/j.ijhydene.2006.11.026>
5. M. Bonanno, K. Müller, B. Bensmann, R. Hanke-Rauschenbach, D. Aili, T. Franken, A. Chromik, R. Peach, A.T.S. Freiberg, and S. Thiele, Review and Prospects of PEM Water Electrolysis at Elevated Temperature Operation. Advanced Materials Technologies. **9**, 2300281 (2024). DOI: 10.1002/admt.202300281
6. L.J.M.J. Blomen, M.N. Mugerwa, Fuel Cell Systems. Springer New York, 1993. DOI 10.1007/978-1-4899-2424-7, ISBN 978-1-4899-2426-1, p. 307.
7. P. Bretzler, E. Christensen, R.W. Berg, N.J. Bjerrum, Pressurized solid phosphate electrolyzer for medium temperature water splitting. Ionics **28**, 3421 (2022). <https://doi.org/10.1007/s11581-022-04532-4>
8. N. Fujiwara, H. Nagase, S. Tada, R. Kikuchi, Hydrogen Production by Steam Electrolysis in Solid Acid Electrolysis Cells. ChemSusChem. **14**, 417 (2021). <https://doi.org/10.1002/cssc.202002281>
9. A.J. Reese, A.J. Peng, A.K. Nason, J. Suntivich, Intermediate-Temperature Electrolysis: Electrode Microstructure and Chemistries. 2022 ECS Meeting Abstracts **MA2022-02**, 1728 (2022). DOI: 10.1149/MA2022-02461728mtgabs
10. Y. Yin, Y. Ying, G. Liu, H. Chen, J. Fan, Z. Li, C. Wang, Z. Guo, G. Zeng, High Proton-Conductive and Temperature-Tolerant PVC-P4VP Membranes towards Medium-Temperature Water Electrolysis. Membranes **12**, 363 (2022). <https://doi.org/10.3390/membranes12040363>
11. S.A. Grigoriev, A.A. Kalinnikov, N.V. Kuleshov and P. Millet, Numerical optimization of bipolar plates and gas diffusion electrodes for PBI-based PEM fuel cells. International Journal of Hydrogen

- Energy **38**, 8557 (2013).  
<https://doi.org/10.1016/j.ijhydene.2012.12.021>
12. A.A. Kalinnikov, S.A. Grigoriev, D.G. Bessarabov, and K. Bouzek, Two-phase mass transfer in porous transport layers of the electrolysis cell based on a polymer electrolyte membrane: Analysis of the limitations. *Electrochim. Acta* **387**, 138541 (2021).  
<https://doi.org/10.1016/j.electacta.2021.138541>
  13. <https://www.fuelcellstore.com/spec-sheets/pSOL-high-temperature-cationic-ionomer-brochure.pdf>
  14. D. Aili, M.K. Hansen, C. Pan, et al. Phosphoric acid doped membranes based on Nafion<sup>®</sup>, PBI and their blends – Membrane preparation, characterization and steam electrolysis testing *International Journal of Hydrogen Energy* **36**, 6985 (2011). doi:10.1016/j.ijhydene.2011.03.058